

The Spin Periods and Magnetic Moments of White Dwarfs in Magnetic Cataclysmic Variables

A.J. Norton

Department of Physics and Astronomy, The Open University, Walton Hall, Milton Keynes MK7 6AA, U.K.

A.J.Norton@open.ac.uk

G.A. Wynn

Astronomy Group, University of Leicester, Leicester LE1 7RH, U.K.

gaw@astro.le.ac.uk

and

R.V. Somerscales

formerly Department of Physics and Astronomy, The Open University, Walton Hall, Milton Keynes MK7 6AA, U.K.

ABSTRACT

We have used a model of magnetic accretion to investigate the rotational equilibria of magnetic cataclysmic variables (mCVs). The results of our numerical simulations demonstrate that there is a range of parameter space in the $P_{\text{spin}}/P_{\text{orb}}$ versus μ_1 plane at which rotational equilibrium occurs. This has allowed us to calculate the theoretical histogram describing the distribution of magnetic CVs as a function of $P_{\text{spin}}/P_{\text{orb}}$. We show that this agrees with the observed distribution assuming that the number of systems as a function of white dwarf magnetic moment is distributed approximately according to $N(\mu_1)d\mu_1 \propto \mu_1^{-1}d\mu_1$. The rotational equilibria also allow us to infer approximate values for the magnetic moments of all known intermediate polars. We predict that intermediate polars with $\mu_1 \gtrsim 5 \times 10^{33}$ G cm³ and $P_{\text{orb}} > 3$ h will evolve into polars, whilst those with $\mu_1 \lesssim 5 \times 10^{33}$ G cm³ and $P_{\text{orb}} > 3$ h will either evolve into low field strength polars which are (presumably) unobservable, and possibly EUV emitters, or, if their fields are buried by high accretion rates, evolve into conventional polars once their magnetic fields re-surface when the mass accretion rate reduces. We

speculate that EX Hya-like systems may have low magnetic field strength secondaries and so avoid synchronisation. Finally we note that the equilibria we have investigated correspond to a variety of different types of accretion flow, including disc-like accretion at small $P_{\text{spin}}/P_{\text{orb}}$ values, stream-like accretion at intermediate $P_{\text{spin}}/P_{\text{orb}}$ values, and accretion fed from a ring at the outer edge of the white dwarf Roche lobe at higher $P_{\text{spin}}/P_{\text{orb}}$ values.

Subject headings: accretion, accretion discs - binaries: close - stars: magnetic fields.

1. Introduction

The magnetic cataclysmic variable stars (mCVs) provide a unique insight into the process of accretion in extreme astrophysical environments. Accretion within these binary stars takes place in the presence of intense magnetic fields and high-energy radiation fields. The mCVs are interacting binary stars in which a magnetic white dwarf (WD) accretes mass from a late-type companion star via Roche lobe overflow. The white dwarfs have very large magnetic moments ($\mu_1 \sim 10^{32} - 10^{35}$ G cm³) and magnetic stresses have a pervasive influence on the accretion dynamics. The mCVs fall into two distinct classes: the AM Herculis stars (or polars) and the intermediate polars (IPs or DQ Herculis stars) (a comprehensive review of mCVs may be found in Warner 1995). The rotational periods of the WDs (P_{spin}) in the AM Her stars are observed to be closely locked to the orbital period (P_{orb}), whereas the WDs within the intermediate polars rotate more rapidly than the orbital period. The period-locking in the AM Her stars, which contain the most strongly magnetic WDs, is thought to come about because the interaction between the magnetic fields of the two stars in the binary is able to overcome the spin-up torque of the accreting matter (see e.g. King, Frank and Whitehurst 1991). This suggests that magnetic effects are important throughout these objects. Indeed, observations of the AM Her stars highlight the unique form of the accretion flow within these binaries, revealing that the gas flow is confined to a stream flowing along magnetic field-lines on to the poles of the WD. The intermediate polars represent the various systems which fill the phase space between the strongly magnetic AM Her stars and the non-magnetic CVs. The accretion flows within IPs are known to take on a wide variety of forms, from magnetized accretion streams to extended accretion discs. This variety has constantly perplexed efforts to understand these objects.

At some point the accretion flow in all mCVs becomes magnetized and forced into field-aligned flow. This magnetized flow reaches the magnetic poles of the primary star at highly ballistic speeds and passes through a strong shock before accreting on to the

WD. The hot, post-shock gas is a source of intense X-ray emission, which is modulated on P_{spin} . Thus, mCVs allow direct observation of the spin rates of the WDs and provide an unparalleled view of the angular momentum distribution within the binaries. Figure 1 shows where the polars and intermediate polars lie in the P_{spin} vs. P_{orb} plane; periods of the intermediate polars are also listed in Table 1. The current census included in the figure contains 67 synchronous polars plus 5 asynchronous polars in which P_{spin} and P_{orb} differ by around 2% or less. These latter systems are assumed to have been disturbed from synchronism by recent nova explosions. Also shown are 39 IPs with a range of properties. Four systems may best be described as nearly synchronous intermediate polars since they have $0.9 \gtrsim P_{\text{spin}}/P_{\text{orb}} \gtrsim 0.7$; a further six systems lie within or below the so-called period gap and have $0.7 \gtrsim P_{\text{spin}}/P_{\text{orb}} \gtrsim 0.07$; whilst another six systems with $P_{\text{spin}}/P_{\text{orb}} \lesssim 0.01$ harbour extremely rapid rotators, including the propeller system AE Aqr and the very long outburst interval SU UMa star, WZ Sge. However, the majority of intermediate polars (currently 23 systems) populate the region defined by $0.25 \gtrsim P_{\text{spin}}/P_{\text{orb}} \gtrsim 0.01$ and $P_{\text{orb}} > 3$ hr. In this paper we use this period distribution to investigate the distribution of magnetic moments of the WDs in mCVs, and the variety of accretion flows that correspond to these equilibrium spin states.

2. Magnetic Accretion Flows

The accretion flow between the two stars in a mCV is ionized by collisions as well as by X-ray irradiation from the strong shock close to the WD surface. Consequently, the accretion flow is highly conducting and its motion relative to the magnetic field of the WD will cause magnetic stresses to alter its dynamics. The equation of motion of the gas in the binary system can be written as

$$\begin{aligned} \frac{\partial \mathbf{v}}{\partial t} + (\mathbf{v} \cdot \nabla) \mathbf{v} &= -\nabla \Phi_R - 2\boldsymbol{\Omega} \wedge \mathbf{v} - \frac{1}{\rho} \nabla P \\ &\quad - \frac{1}{\rho} \nabla \left(\frac{B^2}{8\pi} \right) + \frac{1}{\rho R_c} \left(\frac{B^2}{4\pi} \right) \hat{\mathbf{n}} \end{aligned} \quad (1)$$

where $\boldsymbol{\Omega}$ is the orbital angular velocity, B is the local magnetic field strength, R_c is the local radius of curvature of the magnetic lines of force and Φ_R is known as the Roche potential and includes the effect of both gravitation and centrifugal force. The term $-2\boldsymbol{\Omega} \wedge \mathbf{v}$ is the Coriolis force per unit mass. The magnetic field exerts an isotropic pressure $B^2/8\pi$, and carries a tension $B^2/4\pi$ along the magnetic lines of force. These magnetic stresses act as a barrier to the accretion flow, and impede the motion of plasma across field lines. The details of the flow of plasma through the magnetosphere are complex and non-linear. Its motion is

dynamic and inherently three dimensional, unlike the flow in non-magnetic systems which takes the form a planar disc. The shear velocities between the plasma and the magnetic field are highly supersonic and in some cases can be relativistic. These features, together with the plethora of magnetohydrodynamic instabilities which affect the flow, have made detailed modelling of the accretion process exceedingly difficult.

In general terms we can characterize accretion flow in the presence of a magnetic field by three timescales: $t_{\text{dyn}} \sim (r^3/GM_1)^{1/2}$ is the dynamical timescale of the gas orbit, t_{mag} is the timescale on which magnetic stresses are able to alter the orbital momentum of the accretion flow, and t_{visc} is the timescale on which viscous stresses are able to redistribute angular momentum within the gas flow. We can gain a rough estimate of the extent of the region within which the magnetic field is expected to play an important part in determining the dynamics of the accretion flow (i.e. where $t_{\text{mag}} \lesssim t_{\text{dyn}}$) by comparing the ram pressure of accreting material (ρv^2) and the local magnetic pressure ($B^2/8\pi$). These two quantities are defined to be equal at the Alfvén radius (R_a). Assuming a spherically symmetric accretion flow without significant pressure support we can deduce the spherical Alfvén radius (e.g. Frank, King & Raine 2002)

$$R_a \sim 5.5 \times 10^8 \left(\frac{M_1}{M_{\odot}} \right)^{1/7} R_9^{-2/7} L_{33}^{-2/7} \mu_{30}^{4/7} \text{ cm} \quad (2)$$

where R_9 is the primary radius (in units of 10^9 cm), L_{33} is the system luminosity (in units of 10^{33} erg s $^{-1}$), and μ_{30} is the primary dipole moment (in units of 10^{30} G cm 3). Typically we find that R_a is greater than the system separation (a) in the AM Her stars, and magnetic effects are expected to dominate throughout the binary, as observed.

In the non-magnetic CVs the accretion process is unimpeded by the presence of a magnetic field. The accretion flow leaves the secondary star in the form of a thin stream from its surface (see Warner 1995 for a review of mass transfer via Roche lobe overflow) and adopts a circular, Keplerian orbit at a radius R_{circ} from the WD. An accretion disc forms from the viscous evolution of the stream from R_{circ} in a time t_{visc} .

In the case of a mCV we must consider the effect of the magnetic field on the disc formation process. If $R_a > R_{\text{circ}}$ then we have $t_{\text{mag}}(R_{\text{circ}}) < t_{\text{visc}}(R_{\text{circ}})$, and magnetic stresses will quickly (in a time $< t_{\text{visc}}$) dissipate the stream angular momentum and no accretion disc will form. It is possible to estimate R_{circ} from the conservation of angular momentum: $2\pi b^2/P_{\text{orb}} \sim (GM_1 R_{\text{circ}})^{1/2}$, where b is the distance from the WD to the L_1 point and M_1 is the mass of the WD. This results in the relation

$$\frac{R_{\text{circ}}}{a} \simeq (1+q) \left(\frac{b}{a} \right)^4 \quad (3)$$

which is a function of the mass ratio $q = M_2/M_1$ only, here M_2 is the mass of the donor

star. Typically we find $R_{\text{circ}} \lesssim a/10$ in mCVs. As noted above, $R_a \gg R_{\text{circ}}$ is satisfied in the AM Her stars and no accretion disc can form. In this case we have the hierarchy of timescales $t_{\text{mag}} \lesssim t_{\text{dyn}} \ll t_{\text{visc}}$ at L_1 . In the case of the pulsing X-ray binaries, in which a magnetic neutron star is surrounded by an extensive accretion disc, one finds that $R_a \ll R_{\text{circ}}$ and hence $t_{\text{mag}}(R_{\text{circ}}) \gg t_{\text{visc}}(R_{\text{circ}})$, confirming that accretion disc formation is unaffected by the magnetic field. However, the inward spread of the accretion disc will eventually be halted by the magnetic field at some radius R_{in} . The usual definition of R_{in} is the point at which the magnetic field removes angular momentum from the disc at a greater rate than viscous stresses (e.g. Bath, Evans & Pringle, 1974)

$$-B_\phi B_z R^2|_{R_{\text{in}}} = \dot{M} \frac{d}{dr}(\Omega_K R^2)|_{R_{\text{in}}} \quad (4)$$

where B_ϕ, B_z are the toroidal and poloidal field components respectively, and Ω_K is the Keplerian angular velocity. The value of R_{in} has an important effect on the equilibrium value of P_{spin} , which in turn has an important effect on the dynamics of the accretion flow. In the case of the asynchronous mCVs we find that in many cases $R_a \gtrsim R_{\text{circ}}$, which greatly complicates the accretion dynamics in these systems. A number of models have been put forward in an attempt to explain these systems. The ‘standard’ model of the accretion flow within the intermediate polars assumes them to be the WD analogue of the pulsing X-ray binaries: accreting via an extended accretion disc which is disrupted inside R_{circ} . However it has become clear (e.g. Hellier, 1996) that the intermediate polars represent a variety of different magnetic phenomena. This realization has been prompted by observational techniques such as Doppler tomography, along with new methods for the theoretical treatment of the gas flow within the intermediate polars.

3. Spin Equilibria

Figure 1 shows that the AM Her systems broadly follow the synchronization line along which $P_{\text{spin}} = P_{\text{orb}}$. The asynchronous systems occupy a wide range of parameter space between $10^{-3} \lesssim P_{\text{spin}}/P_{\text{orb}} \lesssim 1$. This fact alone hints at the variety of magnetic flows which are present within these systems.

The spin periods of IPs allow us a unique insight into the angular momentum balance within the binary systems, and are a crucial diagnostic tool when comparing theoretical models. The spin rate of a magnetic WD accreting via a disc reaches an equilibrium when the rate at which angular momentum is accreted by the white dwarf is balanced by the braking effect of the magnetic torque on the disc close to R_{in} . Because of the complex nature of the disc-magnetosphere interaction, most models assume that the system is axisymmetric

and in steady state. Many of these models find that the point at which the accretion disc is disrupted (R_{in}) is very close to the WD co-rotation radius (R_{co}) (e.g. King & Lasota 1991). The radius R_{co} is defined to be the radius at which the magnetic field rotates at the same rate as the local Keplerian frequency, and hence $R_{\text{co}} = (GM_1 P_{\text{spin}}^2 / 4\pi^2)^{1/3}$. The relation $R_{\text{in}} \sim R_{\text{co}}$ implies that a small magnetosphere (low μ_1) results in fast equilibrium rotation and vice versa. Specifically, for a magnetic system with a truncated accretion disc we expect $R_{\text{in}} \sim R_{\text{co}} \ll R_{\text{circ}}$, which translates into the relation $P_{\text{spin}}/P_{\text{orb}} \ll 0.1$. This is certainly satisfied by the pulsing X-ray binaries where $P_{\text{spin}}/P_{\text{orb}} \lesssim 10^{-6}$. Figure 1 clearly shows that some of the asynchronous mCVs also follow this relation. Notably, in GK Per ($P_{\text{spin}} = 381$ s, $P_{\text{orb}} = 48$ hr) P_{orb} is so long that $R_a \ll R_{\text{circ}}$. The other rapidly rotating WDs in the systems close to or below the $P_{\text{spin}} = 0.01P_{\text{orb}}$ line presumably have rather low magnetic fields. It would seem then that some mCVs do indeed conform to the standard model and resemble the pulsing X-ray binaries in accreting via an extended Keplerian disc, which is disrupted close to the WD surface. However it is also clear from the figure that this is not true for all of the systems, as the distribution of spin periods extends out beyond $P_{\text{spin}}/P_{\text{orb}} \gtrsim 0.1$. These systems are unlikely to possess accretion discs, since $P_{\text{spin}}/P_{\text{orb}} \gtrsim 0.1$ implies $R_{\text{in}} \sim R_{\text{co}} \gtrsim R_{\text{circ}}$. King (1993) and Wynn & King (1995) examined the regime in which $t_{\text{mag}}(R_{\text{circ}}) \lesssim t_{\text{dyn}}(R_{\text{circ}})$ utilizing the model detailed in section 4 below. Numerical calculations show that the WD attains a spin equilibrium determined approximately by the condition $R_{\text{co}} \sim R_{\text{circ}}$ corresponding to $P_{\text{spin}}/P_{\text{orb}} \sim 0.1$. The exact value of the equilibrium $P_{\text{spin}}/P_{\text{orb}}$ is dependent on q . In an extension of this analysis King & Wynn (1999) discovered a continuum of spin equilibria which explained the long spin period of EX Hydra ($P_{\text{spin}} = 67$ min, $P_{\text{orb}} = 98$ min; see section 5 below), and linked all of the mCVs in the context of a single model for the first time. The fundamental property of these magnetic accretion flows is the non-Keplerian nature of the velocity field.

The above arguments implicitly assume that the WDs within the asynchronous mCVs are in spin equilibrium. This is expected to be the case as the spin-up/down timescale ($\lesssim 10^7$ y) of the white dwarf is short when compared to the lifetime of the binary ($\gtrsim 10^9$ y), (see e.g. Wynn & King 1995). We also note that in cases where \dot{P}_{spin} is measured for intermediate polars, several are spinning up whilst a similar number are spinning down, and FO Aqr has been seen to do both (e.g. Patterson et al 1998). Hence the assumption that many intermediate polars *are* close to their equilibrium spin periods is a good one with only small deviations apparent on short timescales. However, this is certainly not the case in all of the systems: the very short spin period of AE Aqr ($P_{\text{spin}} = 33$ s, $P_{\text{orb}} = 9.88$ hr) does not imply the presence of a Keplerian accretion disc as the WD is currently a long way from spin equilibrium (Wynn, King & Horne 1997).

4. The Magnetic Model

The equation of motion for gas flow within mCVs (e.g. Equation 1) includes magnetic pressure and tension terms. King (1993) and Wynn & King (1995) constructed a model of accretion flows in the mCVs by assuming that material moving through the magnetosphere interacts with the local magnetic field via a shear-velocity dependent acceleration. This is analogous to the assumption that the magnetic stresses are dominated by the tension term in Equation 1 giving a magnetic acceleration

$$\mathbf{a}_{\text{mag}} \simeq \frac{1}{R_c \rho} \left(\frac{B^2}{4\pi} \right) \hat{\mathbf{n}} \quad (5)$$

Where R_c is local radius of curvature of the magnetic lines of force, B is the local magnetic field strength, and ρ is the local gas density. Because the magnetic tension stresses arise from currents induced by the rotational shear between the plasma flow and the external WD magnetosphere, we can write this acceleration in terms of the velocity shear in the general form

$$\mathbf{a}_{\text{mag}} \simeq -k(r, t, \rho) [\mathbf{v} - \mathbf{v}_f]_{\perp} \quad (6)$$

where \mathbf{v} and \mathbf{v}_f are the velocities of the material and field lines, and the suffix \perp refers to the velocity components perpendicular to the field lines. The coefficient k contains the details of the plasma-magnetic field interaction, and will be a function of position, time and gas density in general. This can be found, at least in approximate form, for the limiting cases of diamagnetic and magnetized accretion flows. Recently, for example, Matthews, Speith & Wynn (2004) used a similar treatment to study the effect of a central magnetic field on the structure of a magnetized accretion disc in the FU Orionis objects. Some of the advantages of this approach are that it simplifies the complex MHD, is easy to add in to hydrodynamic codes, and allows investigation of the spin evolution of WDs in mCVs. The main drawbacks are that some physics is inevitably lost and the k parameter is model dependent. King (1993) and Wynn & King (1995) approximated the plasma flow in mCVs as inhomogeneous and diamagnetic, interacting with the field via a surface drag force characterized by the magnetic timescale

$$t_{\text{mag}} \sim c_A \rho_b l_b B^{-2} \frac{|\mathbf{v}_\perp|}{|\mathbf{v} - \mathbf{v}_f|_\perp} \quad (7)$$

(cf. Equation 10 in Matthews, Speith & Wynn 2004). The k parameter in this case is given by

$$k \sim \frac{B^2}{c_A \rho_b l_b} \sim t_{\text{mag,slow}}^{-1} \quad (8)$$

where c_A is the Alfvén speed in the medium surrounding the plasma, ρ_b is the plasma density and l_b is the typical length-scale over which field-lines are distorted. Here $t_{\text{mag,slow}}$ is

the limiting value of t_{mag} in the case of a slowly rotating WD ($\mathbf{v}_f \rightarrow 0$). The plasma density and length-scale may be approximated by

$$\rho_b \sim \frac{\dot{M}4\pi^2}{P_{\text{orb}}^2 c_s^3} \quad (9)$$

and

$$l_b \sim \frac{P_{\text{orb}} c_s}{2\pi} \quad (10)$$

which are the accretion stream density and width in the vicinity of the L1 point respectively, and c_s is the sound speed. Plasma will exchange orbital energy and angular momentum with the field on the magnetic timescale, which is dependent on P_{spin} since $|\mathbf{v}_f| \sim 2\pi R/P_{\text{spin}}$. Material at radii greater than R_{co} will experience a net gain of angular momentum and be ejected from the binary or captured by the secondary star. On the other hand, material inside R_{co} will lose angular momentum and be accreted by the WD. An equilibrium will result when these angular momentum flows balance. Hence the spin evolution of the WD in mCVs can be followed in detail.

The results presented below were obtained from spin evolution calculations performed using a 3D particle hydrodynamics code using an implementation of the magnetic model described above. The accretion flow calculations were performed in the full binary potential, and included a simple treatment of the gas viscosity. This treatment used a constant viscosity parameter, calibrated to give similar results to a Shakura & Sunyaev parameter of $\alpha \sim 0.01$ for accretion disc formation simulations (i.e. very low k). This value was chosen as appropriate for cold state gas flow (i.e. $\lesssim 10^4$ K as in quiescent dwarf novae discs) which is the expected state of the accretion flow away from the WD surface in mCVs. The reader is referred to Wynn & King (1995, and references therein) for further details on this code.

5. Results

The magnetic model has been used to explore a wide range of IPs parameterized by their orbital period ($P_{\text{orb}} = 80$ min to 10 hours) and magnetic field strength ($k = (10^2 - 10^7)(2\pi/P_{\text{orb}})\text{s}^{-1}$), using $M_1 = 0.7M_{\odot}$ and $M_2 = 0.35M_{\odot}$ (i.e. $q = 0.5$). The mass transfer rate and WD moment of inertia were chosen to facilitate progress towards the equilibrium spin state. All models assume a dipolar structure for the WD magnetic field.

The equilibrium spin periods we have determined are shown by the small dots in Figure 2. Here the k values have been converted into the corresponding value of the white dwarf surface magnetic moment μ_1 using Equations (8), (9) and (10) above. Lines on Figure 2 connect the dots for each orbital period. The line for $P_{\text{orb}} = 80$ m is similar to that obtained

by King & Wynn (1999) for EX Hya, although here calculated for a different mass ratio. It should be noted that there is some latitude in applying the conversion from k to μ_1 , so the envelope of equilibrium periods may shift laterally in the plane. Nonetheless it is encouraging that the predicted equilibrium spin periods lie in the range at which many mCVs are seen. It should also be noted that the estimated magnetic field strengths for the intermediate polars that display polarized emission (e.g. PQ Gem, BG CMi, V2400 Oph and LS Peg) lie within the region covered by the results.

The primary source of uncertainty associated with the equilibrium spin periods in Figure 2 is q . Broadly speaking, the overall shape of the envelope encompassed by the curves on Figure 2 is independent of q . However, the curves shift vertically in the figure with changes in the mass ratio. The reason for this can be seen from the dependence

$$\frac{P_{\text{spin}}}{P_{\text{orb}}} \propto \left(\frac{b}{a}\right)^{3/2} \propto (0.500 - 0.227 \log q)^{3/2} \quad (11)$$

which can be deduced from Equation 3 (see also Equation 13 in King & Wynn 1999). This relation predicts a variation in the predicted equilibrium spin values of $\lesssim 40\%$ when considering the extremes of the expected mass ratio range in CVs ($0.1 \lesssim q \lesssim 0.9$). For mass ratios between the more conservative limits of $0.3 \lesssim q \lesssim 0.7$, the variation in the predicted equilibrium spin period is only of order 10%. These results are borne out to a high degree of accuracy by numerical calculation.

If we now assume that all mCVs are at their equilibrium spin period we can place the intermediate polars on Figure 2 by tracing across at the appropriate $P_{\text{spin}}/P_{\text{orb}}$ value to intersect the equilibrium line for the appropriate orbital period. In this way, most of the squares have been placed on Figure 2. By doing this we ‘predict’ a value for the surface magnetic moment μ_1 of the white dwarf in each system; and these values are listed in Table 1. Given the latitude in converting from k to μ_1 , and also the dependence of the location of these curves on q , we emphasize that these μ_1 values should only be relied upon as an order of magnitude indication of the value in each case.

We note here that since our results were all obtained with $q = 0.5$, they preclude fitting the exact spin states of individual systems in detail. For example, the spin period of EX Hya lies above all of the equilibrium curves we present. However, King & Wynn (1999) were able to fit the spin of EX Hya with an identical model, but using the system parameters specific to that object. The principal difference between the parameters they adopted and the ones we used here is the difference in the mass ratio of the system. The consequent difference in equilibrium spin period can be predicted from the discussion presented above. The mass

ratio of EX Hya is $q = 0.17^{+0.08}_{-0.07}$ (Beuermann et al 2003), so Equation (11) yields the relation

$$\left(\frac{P_{\text{spin}}}{P_{\text{orb}}}\right)_{q=0.17} \simeq 1.30^{+0.15}_{-0.11} \left(\frac{P_{\text{spin}}}{P_{\text{orb}}}\right)_{q=0.5} \quad (12)$$

Since $(P_{\text{spin}}/P_{\text{orb}})_{q=0.5} \sim 0.54$ from our results, we predict $(P_{\text{spin}}/P_{\text{orb}})_{q=0.17} \sim 0.70^{+0.08}_{-0.06}$ for EX Hya, which is indeed consistent with what is observed and the result of King and Wynn (1999).

For the four nearly synchronous intermediate polars that have $P_{\text{spin}}/P_{\text{orb}} \gtrsim 0.7$ we have simply placed them on Figure 2 above the mid-point of the plateau part of the relevant curves at the appropriate $P_{\text{spin}}/P_{\text{orb}}$ value. If these systems are in equilibrium, a similar argument to that used for EX Hya shows that they would have extremely low mass ratios ($q \lesssim 0.15$). For this reason, we prefer to identify these systems as being out of equilibrium and heading towards synchronism.

In the envelope of allowed parameter space shown on Figure 2, we note that the region with $P_{\text{spin}}/P_{\text{orb}} \lesssim 0.1$ corresponds to $R_{\text{mag}} \sim R_{\text{co}} \lesssim R_{\text{circ}}$ and so indicates regions where truncated accretion discs are likely to form. In fact, for $P_{\text{spin}}/P_{\text{orb}} \lesssim 0.1$ the magnetic model shows that equilibrium spin periods do indeed produce accretion flows that are disc-like in nature, whereas for $0.1 \lesssim P_{\text{spin}}/P_{\text{orb}} \lesssim 0.5$ stream-like accretion is the preferred mode. Figure 3 shows examples of some of these accretion flows, corresponding to different regions of the equilibrium parameter space. At even higher period ratios of $P_{\text{spin}}/P_{\text{orb}} \gtrsim 0.5$, we find solutions in which the accretion is fed from a ring-like structure at the outer edge of the WD Roche lobe (Figure 3). This mode of accretion flow is apparent in the upper plateau region of the curves shown in Figure 2 and corresponds to the situation $R_{\text{mag}} \sim R_{\text{co}} \sim b$. We note that this is an additional solution to that found by King & Wynn (1999) for EX Hya. In their solution, systems undergo alternate phases of accretion and ejection to maintain equilibrium whilst fed from a stream. In the solution we have found here, angular momentum from the white dwarf is passed back to the accreting material and some of this material is lost from the outer edge of the ring to maintain equilibrium. This ring-fed solution may be preferred over the stream-fed accretion/ejection solution when the angle between the magnetic dipole axis and the spin axis is small. In fact, the ring-fed solution may be more consistent with the observational data on EX Hya than King & Wynn’s previous solution, since some observations do indeed show evidence for material circling the white dwarf in that system.

6. Synchronisation

We now use the results obtained above to investigate the polar synchronisation condition. We may assume that systems become synchronised once the magnetic locking torque

is equal to the accretion torque. Hence

$$\frac{\mu_1\mu_2}{a^3} = \dot{M}(GM_1R_{\text{mag}})^{1/2} \quad (13)$$

where the surface magnetic moment on the secondary may be approximated by

$$\mu_2 = 2.8 \times 10^{33} P_{\text{orb}}^{9/4} \text{ G cm}^3 \quad (14)$$

from Warner (1996) with P_{orb} in hours. The magnetospheric radius is approximated by the co-rotation radius,

$$R_{\text{mag}} \sim R_{\text{co}} = \left(\frac{GM_1 P_{\text{spin}}^2}{4\pi^2} \right)^{1/3} \quad (15)$$

and the mass accretion rate \dot{M} is set to the secular value given by

$$\dot{M} = 2.0 \times 10^{-11} \times P_{\text{orb}}^{3.7} \text{ M}_\odot \text{ yr}^{-1} \quad (16)$$

for $P_{\text{orb}} > 2.7$ h (McDermott & Taam 1989) and

$$\dot{M} = 2.4 \times 10^{15} \times \frac{M_1^{2/3} P_{\text{orb}}^{-1/6}}{\left(1 - \frac{15q}{19}\right) (1+q)^{1/3}} \text{ g s}^{-1} \quad (17)$$

for angular momentum loss by gravitational radiation (Warner 1995) which we assume to be dominant at $P_{\text{orb}} < 2.7$ h.

Solutions to Equation 13 are plotted as diagonal lines on Figure 4. Each line connects points at which synchronisation will occur for a given orbital period. The lines shown are for orbital periods of 3 h, 4 h, ... 10 h, as those for shorter orbital periods lie to the upper left of the region plotted. Where these diagonal lines intersect the equilibrium spin period lines for their respective orbital periods, gives the points at which systems will synchronize. The locus of these points is shown by the thick line which simply connects the various intersection points. Hence, systems lying below the thick line will not be prone to synchronize, whilst those lying above will tend to do so.

7. Predictions

From Figures 2 and 4 it can be seen that the intermediate polars above the period gap virtually all lie *below* the synchronisation line. The two systems just above the line are RR Cha and RXJ0944.5+0357 with $P_{\text{spin}}/P_{\text{orb}}$ of 0.161 and 0.168 respectively. We suggest these two are probably normal intermediate polars and within the errors of our calculation are

consistent with sitting below the synchronisation line. Lying well above the synchronisation line are the two nearly synchronous intermediate polars V697 Sco and HS0922+1333 with $P_{\text{spin}}/P_{\text{orb}}$ of 0.737 and 0.882 respectively. As noted above, we suggest that these two systems are on their way to synchronism. A similar fate should hold for the rest of the intermediate polars above the period gap that have relatively high white dwarf magnetic moments.

At short orbital periods, the picture is rather different. First, we note that there is a relative dearth of systems here. The number of non-magnetic CVs above the period gap is comparable to the number below it (Ritter & Kolb 2003), yet there are at least four times as many intermediate polars above the gap as below it. We suggest that the original evolutionary arguments for magnetic CVs were probably correct – the majority of intermediate polars do indeed evolve to synchronism and become polars, so explaining why there are so few intermediate polars at short orbital periods. All 6 of the intermediate polars that are observed below or within the period gap ('EX Hya-like systems'), plus the two nearly synchronous intermediate polars RXJ0524+42 and V381Vel, lie above the synchronisation line and so *should* be synchronized. We suggest the reason for them not being so is simply that the secondary stars in the EX Hya-like systems have low magnetic moments (i.e. less than predicted by Equation 14) and so are unable to come into synchronism. They therefore represent the low magnetic field tail-end of a distribution.

It is also apparent from Figure 2 that virtually all the intermediate polars have $\mu_1 \lesssim 5 \times 10^{33}$ G cm³ whereas virtually all the polars have $\mu_1 \gtrsim 5 \times 10^{33}$ G cm³. This discrepancy between the intermediate polar and polar magnetic fields has been noted in the past and was a reason for rejecting the hypothesis of polars evolving into intermediate polars. It also poses the question: where are the synchronous systems with low white dwarf magnetic moments? We can suggest two possibilities for the answer. Firstly, it may be that when the systems with a low white dwarf magnetic moment reach a synchronous state they become primarily EUV emitters and so are unobservable. Secondly there is the possibility raised by Cumming (2002) that the magnetic fields in intermediate polars are buried by their high accretion rate and so are not really as low as they appear. In this picture, as intermediate polars evolve towards shorter orbital periods, mass transfer shuts off when they reach the period gap, the magnetic field of the white dwarf re-surfaces, and the systems synchronize before re-appearing below the period gap as conventional, high field, polars.

8. The magnetic moment distribution of WDs in mCVs

The results shown in Figure 4 can also be used to characterize the theoretical distribution of mCVs as a function of the white dwarf surface magnetic moment. We assume that the

number of systems varies according to

$$N(\mu_1) d\mu_1 \propto \mu_1^{-n} d\mu_1 \quad (18)$$

where n is a number to be determined. We may integrate under the equilibrium curves shown in Figure 4 to get the predicted number of systems within a given range of $P_{\text{spin}}/P_{\text{orb}}$. The number in a given bin is then

$$N \propto \left[\frac{\mu_1^{1-n}}{1-n} \right]_{\mu_1 + \frac{\Delta P_{\text{spin}}}{G P_{\text{orb}}}}^{\mu_1} \quad (19)$$

where G is the gradient of the equilibrium curves in Figure 4 at any point. The range of spin to orbital period ratios was divided into eight logarithmic bins, seven of which were 0.25 wide in log space and the eighth corresponded to synchronous systems. The integration was carried out over the magnetic moment range $10^{32} \text{ G cm}^3 < \mu_1 < 10^{35} \text{ G cm}^3$ and at the spin to orbital period ratio (for a given orbital period) indicated by the thick line in Figure 4, we assume that systems become synchronized. The predicted number of systems was averaged over orbital periods of 3, 4, 5, and 6 hours assuming systems to be distributed evenly in orbital period, and the final result was normalized to the number of known mCVs with orbital periods greater than 3 h.

The best fit value of the power law index n was found to be at 1.10, with a reduced chi-squared of $\chi_r^2 = 0.44$, as shown in Figure 5, although values between ~ 0.95 and 1.27 are also valid ($\chi_r^2 < 1$). The cumulative histograms comparing the observed number of systems with that predicted by Equation 18 with $n = 1.10$ are shown in Figure 6, and the data are listed in Table 2. A power law index of $n \sim 1$ indicates roughly equal numbers of systems per decade of magnetic moment.

9. Testing the applicability of the model

As we have demonstrated, our magnetic model currently evolves systems to their equilibrium spin period and allows examination of the resulting accretion flow. In order to assess the validity of the model, and how accurately it reproduces accretion flows seen in real IPs, it is necessary to test the observable consequences of these results against real data. One such test will be to investigate which of the model flows can support dwarf nova instabilities, evidence for which is seen in a few IPs. We also plan to extend the scope of the model in order to produce synthetic observables which can then be compared with, or fitted to, the wealth of existing data on individual systems. One part of this approach will be to produce synthetic X-ray lightcurves and power spectra, the other will be to produce synthetic optical Doppler tomograms and trailed spectra.

The model explicitly tracks the position and velocity of each diamagnetic blob from the L1 point down to the WD surface. It is therefore already possible to output the mass accretion rate onto a given pole as a function of time, and this capability was illustrated in our recent discussion of RXJ1914.4+2456 and RXJ0806.3+1527 as face-on, stream-fed IPs (Norton, Haswell & Wynn 2004). But this is *not* the same as predicting the X-ray lightcurve. The construction of synthetic X-ray lightcurves from the position and velocity information as a function of time for the accreting material will firstly involve modelling the spectrum and intensity of X-ray emission of an individual blob as it undergoes a shock in the vicinity of the WD surface. The next step will be to perform a ‘ray tracing’ operation to track back the X-ray emission along the line of sight, accounting for occultation of the emission as well as photoelectric absorption and electron scattering in the intervening blobs. By summing the emission from all blobs and allowing the system to evolve in time, synthetic lightcurves (and hence power spectra) can be built up exhibiting variation as a function of white dwarf spin phase, binary phase, and beat phase, all as a function of X-ray energy.

We can also use the accretion flows produced by the model to generate synthetic maps of optical emission by assigning a dissipation rate to each particle in the flow. Since we already know the velocity of each particle, such emission maps can then be converted into synthetic optical trailed spectra, phased both with the spin and orbital periods of a given system. The synthetic trailed spectra can then be converted into synthetic Doppler tomograms i.e. maps of the emission in velocity space, for comparison with observational data.

10. Conclusions

We have demonstrated that there is a range of parameter space in the $P_{\text{spin}}/P_{\text{orb}}$ versus μ_1 plane at which spin equilibrium occurs for mCVs. At equilibrium, with a mass ratio of $q = 0.5$, for $P_{\text{spin}}/P_{\text{orb}} \lesssim 0.1$ accretion is via a truncated accretion disc; for $0.1 \lesssim P_{\text{spin}}/P_{\text{orb}} \lesssim 0.5$ stream-fed accretion occurs; whilst for $P_{\text{spin}}/P_{\text{orb}} \gtrsim 0.5$ accretion may be fed from a ring at the outer edge of the WD Roche lobe. Varying the mass ratio shifts the boundaries of these types of behaviour by of order ten percent, but the overall pattern remains the same.

Using the results of numerical simulations we can infer the surface magnetic moments of the white dwarfs in intermediate polars to be mostly in the range $10^{32} \text{ G cm}^3 \lesssim \mu_1 \lesssim 5 \times 10^{33} \text{ G cm}^3$. Most of the intermediate polars with orbital periods greater than 3 h lie below the synchronisation line, whilst most systems with orbital periods less than 2 h lie above it and should be synchronized. High magnetic moment intermediate polars at long orbital periods will evolve into polars. Low magnetic moment intermediate polars at long orbital periods will either: evolve into low field strength polars which are (presumably) unobservable,

and possibly EUV emitters; or, if their fields are buried by high accretion rates, evolve into conventional polars once their magnetic fields re-surface when the mass accretion rate reduces. EX Hya-like systems may represent the tail end of a distribution such that they have low magnetic field strength secondaries and so avoid synchronisation.

We have also shown that the distribution of mCVs above the period gap follows the relationship $N(\mu_1)d\mu_1 \propto \mu_1^{-1}d\mu_1$, indicating roughly equal numbers of systems per decade of magnetic moment. For comparison, recent data from the Sloan Digital Sky Survey (Schmidt et al 2003), concerning the magnetic field strength distribution of isolated white dwarfs, reveals 38 systems with $10^6 < B/G < 10^7$, 49 systems with $10^7 < B/G < 10^8$ and 20 systems with $10^8 < B/G < 10^9$.

Future work will assess the validity of the accretion flows we have simulated by comparing synthetic observables generated from these flows with the wealth of existing data on individual systems.

11. Acknowledgements

This research has made use of computing facilities in the Open University Department of Physics and Astronomy which are funded by the OU Research Development Fund and Capital Equipment Fund, and supported by PPARC grant PPA/G/O/2000/00037. Theoretical astrophysics at Leicester is supported by a PPARC rolling grant.

REFERENCES

Abbott, T.M.C., Shafter, A.W. 1997, ASP Conf. Ser. 121, 679

Allan, A., Hellier, C., Beardmore, A.P. 1998, MNRAS, 295, 167

Bath, G.T., Evans, W.D., Pringle, J.E. 1974, MNRAS 166, 113

Beuermann, K., Harrison, T.E., McArthur, B.E., Benedict, G.F., Gänsicke, B.T. 2003, AA, 412, 821

Buckley, D.A.H., Haberl, F., Motch, C., Pollard, K., Schwarzenberg-Czerny, A., Sekiguchi, K. 1997, MNRAS, 287, 117

Burwitz, V., Reinsch, K., Beuermann, K., Thomas, H.C. 1996, AA, 310, L25

Choi, C.S., Dotani, T., Agrawal, P.C. 1999, ApJ, 525, 399

Cumming, A. 2002, MNRAS, 333, 589

de Martino, D., Mouchet, M., Bonnet-Bidaud, J.M., Vio, R., Rosen, S.R., Mukai, K., Augusteijn, T., Garlick, M.A. 1995, AA, 298, 849

de Martino, D., Silvotti, R., Buckley, D.A.H., Gänsicke, B., Mouchet, M., Mukai, K., Rosen, S.R. 1999, AA, 350, 517

de Martino, D., Matt, G., Mukai, K., Belloni, T., Bonnet-Bidaud, J.M., Chiappetti, L., Gänsicke, B.T., Haberl, F., Mouchet, M. 2001, AA, 377, 499

Duck, S.R., Rosen, S.R., Ponman, T.J., Norton, A.J., Watson, M.G., & Mason, K.O. 1994, MNRAS, 271, 372

Frank J., King A.R., Raine D.J. 2002, Accretion power in astrophysics, 3rd edn. Cambridge Univ. Press, Cambridge

Haberl, F., Motch, C., Zickgraf, F.J. 2002, AA, 387, 201

Harlaftis, E., Horne, K. 1999, MNRAS, 305, 437

Haswell, C.A., Patterson, J., Thorstensen, J.R., Hellier, C., & Skillman, D.R. 1997, ApJ, 476, 847

Hellier, C., Mukai, K., Beardmore, A.P. 1997, MNRAS, 292, 397

Hellier, C., Beardmore, A.P., Mukai, K. 2002, AA, 389, 904

Hellier, C., Wynn G.A., Buckley, D.A.H. 2002, MNRAS, 333, 84

Kemp, J., Patterson, J., Thorstensen, J.R., Fried, R.E., Skillman, D.R., Billings G. 2002, PASP, 114, 623

King A.R. 1993, MNRAS 261, 144

King, A.R., Lasota, J-P. 1991, ApJ, 378, 674

King, A.R., Frank, J., Whitehurst, R. 1991, MNRAS 250, 152

King, A.R., Wynn, G.A. 1999, MNRAS 310, 203

Matthews, O.M., Speith, R., Wynn, G.A., 2004, MNRAS, 347, 873

McDermott, P.N., Taam, R.E. 1989, ApJ 342, 1019

Morales-Rueda, L., Still, M.D., Roche, P. 1996, MNRAS, 283, 58

Norton, A.J., Hellier, C., Beardmore, A.P., Wheatley, P.J., Osborne, J.P., Taylor, P. 1997, MNRAS, 289, 362

Norton, A.J., Quaintrell, H., Katajainen, S., Lehto, H.J., Mukai, K., Negueruela, I. 2002, AA, 384, 195

Norton, A.J., Haswell, C.A., Wynn, G.A. 2004, AA, 419, 1025

Patterson, J., Kemp, J., Richman, H.R., Skillman, D.R., Vanmunster, T., Jensen, L., Buckley, D.A.H., O'Donoghue, D., Kramer, R., 1998, PASP, 110, 415

Retter, A., Leibowitz, E.M., Kovo-Kariti, O. 1998, MNRAS, 293, 145

Ritter, H., Kolb, U. 2003, AA, 404, 301

Rodriguez-Gil, P., Casares, J., Martinez-Pais, I.G., Hakala, P., & Steeghs, D. 2001, ApJ, 548, L49

Rodriguez-Gil, P., Casares, J., Martinez-Pais, I.G., Hakala, P.J. 2002, ASP Conf. Ser., 261, 533

Schmidt, G.D., et al 2003, ApJ, 595, 1101

Schwarz, R. 2004, in Cropper, M., Vrielmann, S., eds., Magnetic cataclysmic variables, ASP conference series, Proc. IAU Colloq. 190

Schwope, A.D., Catalan, M.S., Beuermann, K., Metzner, A., Smith, R.C., Steeghs, D. 2002, MNRAS 313, 533

Staude, A. Schwope, A.D., Krumpe, M., Hambaryan, V., Schwarz, R. 2003, AA, 406, 253

Taylor, P., Beardmore, A.P., Norton, A.J., Osborne, J.P., Watson, M.G. 1997, MNRAS, 289, 349

Thorstensen, J.R., Taylor, C.J. 2000, MNRAS, 312, 629

Tovmassian, G. 2004, in Cropper, M., Vrielmann, S., eds., Magnetic cataclysmic variables, ASP conference series, Proc. IAU Colloq. 190

Vrtilek, S.D., Silber, A., Primini, F., Raymond, J.C. 1996, ApJ, 465, 951

Warner, B. 1995, Cataclysmic Variable Stars, Cambridge Univ. Press, Cambridge

Warner, B. 1996, *Astrophysics & Space Science* 241, 263

Warner, B., Woudt, P.A. 2002, *PASP*, 114, 1222

Welsh, W.F., Sion, E.M., Godon, P., Gänsicke, B.T., Knigge, C., Long, K.S., Szkody, P. 2003, *APJ*, 599, 509

Woudt, P.A., Warner, B. 2002, *MNRAS*, 335, 44

Woudt, P.A., Warner, B. 2003a, *MNRAS*, 339, 731

Woudt, P.A., Warner, B. 2003b, *MNRAS*, 340, 1011

Woudt, P.A., Warner, B. 2004, in Cropper, M., Vrielmann, S., eds., *Magnetic cataclysmic variables*, ASP conference series, Proc. IAU Colloq. 190

Wynn G.A., King A.R. 1995, *MNRAS* 275, 9

Wynn G.A., King A.R., Horne, K. 1997, *MNRAS* 286, 436

Zhang, E., Robinson, E.L., Stiening, R.F., Horne, K. 1995, *ApJ*, 454, 447

Table 1. Intermediate polars with known spin and orbital periods

Star	X-ray name	P_{spin}/s	P_{orb}/h	$P_{\text{spin}}/P_{\text{orb}}$	Inferred $\mu_1/\text{G cm}^3$	Period Ref.
Rapid rotators						
WZ Sge		28.96	1.3606	0.0572	$< 10^{32}$	1
AE Aqr	1E2037.5-0102	33.0767	9.87973	0.00093	$< 10^{32}$	2
GK Per	3A0327+438	351.341	47.9233	0.00204	$< 10^{32}$	3
V533 Her		63.633	3.53	0.00501	$< 10^{32}$	4
DQ Her		142	4.6469	0.00849	$< 10^{32}$	5
XY Ari	H0253+193	206.30	6.0648	0.00945	4.5×10^{32}	6
Regular IPs, $P_{\text{orb}} > 3\text{h}$						
V709 Cas	RXJ0028.8+5917	312.8	5.34	0.0163	4.2×10^{32}	7
	1RXSJ1548-4528	693	6.72/9.37	0.0286/0.0205	$1.0/1.4 \times 10^{33}$	8
2236+0052		403.7	3.23	0.0347	2.6×10^{32}	9
V405 Aur	RXJ0558.0+5353	545	4.15	0.0365	4.8×10^{32}	10
YY Dra	3A1148+719	529.31	3.96898	0.0370	4.7×10^{32}	11
PQ Gem	2REJ0751+144	833.411	5.1927	0.0446	8.3×10^{32}	12
V1223 Sgr	4U1849-31	745.506	3.36586	0.0615	4.0×10^{32}	13
AO Psc	H2252-035	805.203	3.59105	0.0623	5.2×10^{32}	13
HZ Pup		1212.2	5.11	0.0659	9.1×10^{32}	14
UU Col	RXJ0512.2-3241	863.5	3.45	0.0695	6.5×10^{32}	15
	1RXSJ062518.2+733433	1187.244	4.71863	0.0699	1.0×10^{33}	16
FO Aqr	H2215-086	1254.451	4.84944	0.0718	1.2×10^{33}	17
V2400 Oph	RXJ1712.6-2414	927	3.41	0.0755	1.1×10^{33}	18
BG CMi	3A0729+103	913.496	3.23397	0.0785	1.2×10^{33}	19
TX Col	H0542-407	1911	5.718	0.0928	4.0×10^{33}	20
	1WGA1958.2+3232	1466.66	4.35	0.0937	2.5×10^{33}	21
TV Col	3A0527-329	1910	5.48641	0.0967	4.1×10^{33}	22
AP Cru		1837	5.12	0.0997	3.7×10^{33}	23
V1062 Tau	H0459+246	3726	9.952	0.104	1.4×10^{34}	24
LS Peg		1776	4.19	0.118	3.4×10^{33}	25
RR Cha		1950	3.37	0.161	3.4×10^{33}	23
	RXJ0944.5+0357	2162	3.58	0.168	4.0×10^{33}	9
V1425 Aql		5188	6.14	0.235	1.8×10^{34}	26
EX Hya-like IPs, $P_{\text{orb}} < 3\text{h}$						
DD Cir		670	2.34	0.080	1.7×10^{32}	27
HT Cam	RXJ0757.0+6306	511	1.35	0.105	2.7×10^{32}	28
V795 Her		1172	2.60	0.125	3.6×10^{32}	29
	RXJ1039.7-0507	1444	1.574	0.255	9.2×10^{32}	30
V1025 Cen	RXJ1238-38	2147	1.42	0.420	1.8×10^{33}	31
EX Hya	4U1249-28	4021.62	1.637612	0.682	$\sim 5 \times 10^{33}$	32
Nearly synchronous IPs						
V697 Sco		11916	4.49	0.737	$> 1 \times 10^{35}$	33
HS0922+1333		14636.16	4.608	0.882	$> 1 \times 10^{35}$	34
	RXJ0524+42	8160	2.617	0.866	$> 1 \times 10^{34}$	35
V381 Vel		7320	2.233	0.910	$> 1 \times 10^{34}$	34

References. — (1) Welsh et al 2003; (2) Choi, Dotani & Agrawal 1999; (3) Morales-Rueda, Still & Roche 1996; (4) Thorstensen & Taylor 2000; (5) Zhang et al 1995; (6) Hellier, Mukai & Beardmore 1997; (7) de Martino et al 2001; (8) Haberl, Motch & Zickgraf 2002; (9) Woudt & Warner 2004; (10) Harlaftis & Horne 1999; (11) Haswell et al 1997; (12) Duck

et al 1994; (13) Taylor et al 1997; (14) Abbott & Shafter 1997; (15) Burwitz et al 1996; (16) Staude et al 2003; (17) de Martino et al 1999; (18) Buckley et al 1997; (19) de Martino et al 1995; (20) Norton et al 1997; (21) Norton et al 2002; (22) Vrtilek et al 1996; (23) Woudt & Warner 2002; (24) Hellier, Beardmore & Mukai 2002; (25) Rodriguez-Gil et al 2001; (26) Retter, Leibowitz & Kovo-Kariti 1998; (27) Woudt & Warner 2003b; (28) Kemp et al 2002; (29) Rodriguez-Gil et al 2002; (30) Woudt & Warner 2003a; (31) Hellier, Wynn & Buckley 2002; (32) Allan, Hellier & Beardmore 1998; (33) Warner & Woudt 2002; (34) Tovmassian 2003; (35) Schwarz 2003.

Table 2. Histograms comparing the observed number of systems with that predicted by Equation 18 with $n = 1.10$. The first two columns indicate the lower edge of the bins.

$\log(P_{\text{spin}}/P_{\text{orb}})$	$P_{\text{spin}}/P_{\text{orb}}$	$N(\text{obs})$	$N(\text{model})$
-2.00	0.010	1	0.44
-1.75	0.018	1	0.72
-1.50	0.032	4	1.34
-1.25	0.056	12	17.77
-1.00	0.100	4	1.74
-0.75	0.178	1	1.26
-0.50	0.316	0	0.32
-0.25	0.562	2	0.00
0.00	1.000	26	27.41

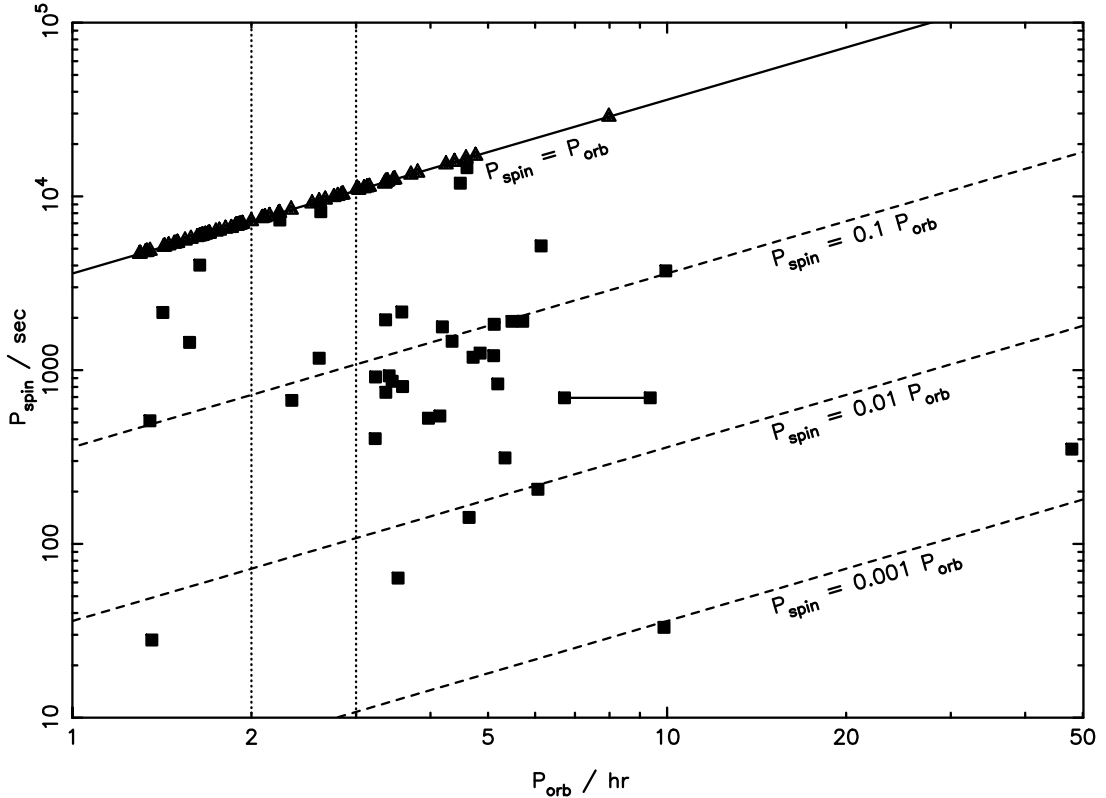


Fig. 1.— The spin and orbital periods of the mCVs. Polars are indicated by triangles and intermediate polars by squares. The four ‘nearly synchronous’ IPs (i.e. $0.9 > P_{\text{spin}}/P_{\text{orb}} > 0.7$) are V697 Sco, HS0922+1333, RX J0425+42 and V381 Vel; the six ‘rapid rotators’ shown (i.e. $P_{\text{spin}}/P_{\text{orb}} < 0.01$) are WZ Sge, AE Aqr, GK Per, V533 Her, DQ Her and XY Ari; the six conventional IPs within or below the period gap are DD Cir, HT Cam, V795 Her, RX J1039.7–0507, V1025 Cen and EX Hya. The remaining 23 conventional IPs above the period gap are V709 Cas, 1RXSJ154814.5–452845, 2236+0052, V405 Aur, YY Dra, PQ Gem, V1223 Sgr, AO Psc, HZ Pup, UU Col, 1RXSJ062518.2+733433, FO Aqr, V2400 Oph, BG CMi, TX Col, 1WGA1958.2+3232, TV Col, AP Cru, V1062 Tau, LS Peg, RR Cha, RXJ0944.5+0357 and V1425 Aql. See also Table 1.

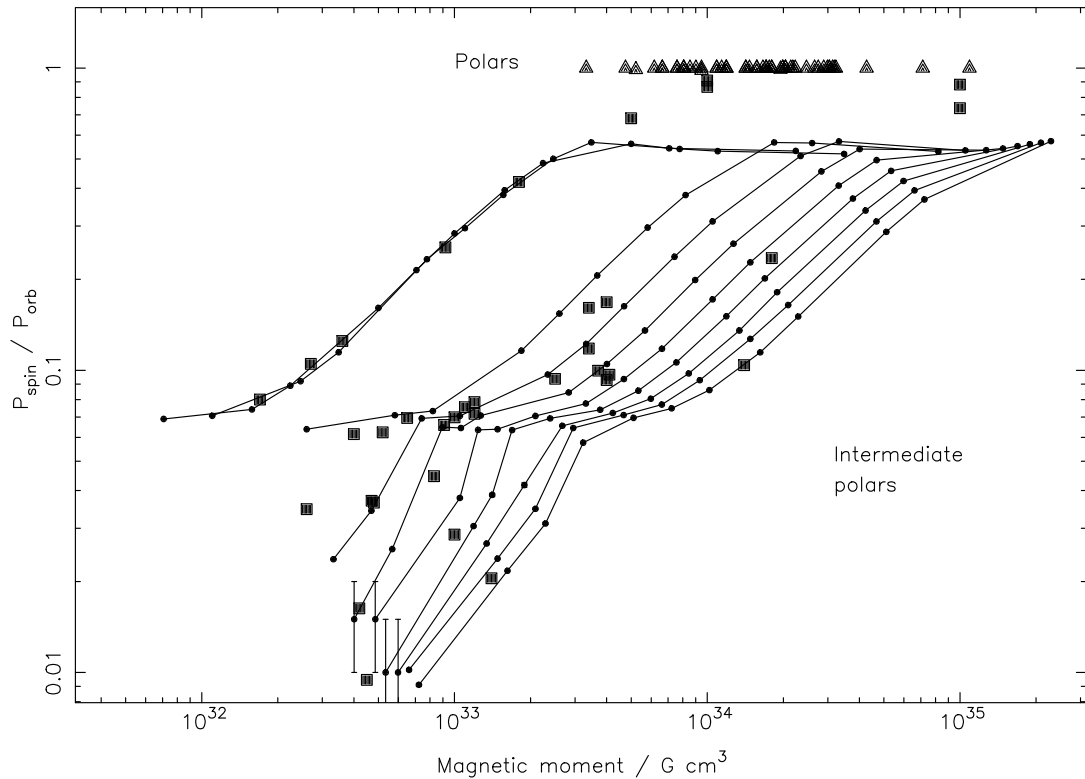


Fig. 2.— The equilibrium spin periods of mCVs obtained by running the model. Each line connects a set of data points corresponding to different k values and represents the equilibrium spin periods at a given orbital period. The ten lines correspond to orbital periods of 80 m, 2 h, 3 h ... 10 h. In general the uncertainty in each equilibrium spin period is smaller than the size of the plotted point, except for a few of the points at the lower extreme of the lines, where indicative error bars are shown. The measured magnetic moments of polars are shown by the triangles along the top of the figure. The estimated magnetic moments of the intermediate polars are shown by squares and have been obtained by tracing across at the appropriate $P_{\text{spin}}/P_{\text{orb}}$ value to intersect the equilibrium line for the appropriate orbital period.

Fig. 3.— Examples of the accretion flows at equilibrium for $P_{\text{orb}} = 4$ hr. The top row shows side-on views of the system, the bottom row shows the same system in a face-on view. The left panels have $k = 500$ and correspond to $P_{\text{spin}}/P_{\text{orb}} = 0.07$ and $\mu_1 \sim 7 \times 10^{32} \text{ G cm}^3$; the middle panels have $k = 50000$ and correspond to $P_{\text{spin}}/P_{\text{orb}} = 0.24$ and $\mu_1 \sim 7 \times 10^{33} \text{ G cm}^3$; whilst the right panels have $k = 10^7$ and correspond to $P_{\text{spin}}/P_{\text{orb}} = 0.53$ and $\mu_1 \sim 10^{35} \text{ G cm}^3$. Truncated disc-like flows occur for lower magnetic moments at $P_{\text{spin}}/P_{\text{orb}} < 0.1$; stream-like flows occur for higher magnetic moments at $0.1 < P_{\text{spin}}/P_{\text{orb}} < 0.5$ and accretion fed from a ring-like structure at the outer edge of the WD Roche lobe occurs for the highest magnetic moments at $P_{\text{spin}}/P_{\text{orb}} > 0.5$.

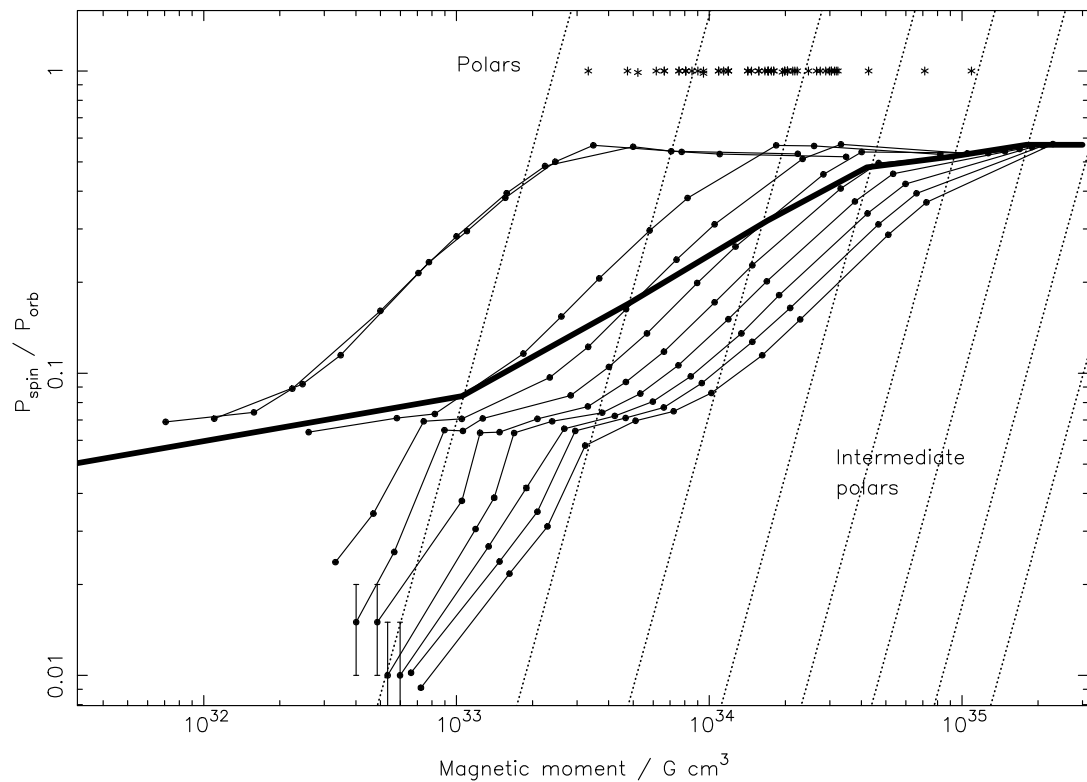


Fig. 4.— Diagonal lines show solutions to Equation 13 for orbital periods 3 h, 4 h, ... 10 h. The lines for shorter orbital periods are to the upper left of the region plotted. Where these diagonal lines intersect the equilibrium spin period lines for their respective orbital periods, gives the points at which systems will synchronize. The locus of these points is shown by the thick line which simply connects the various intersection points.

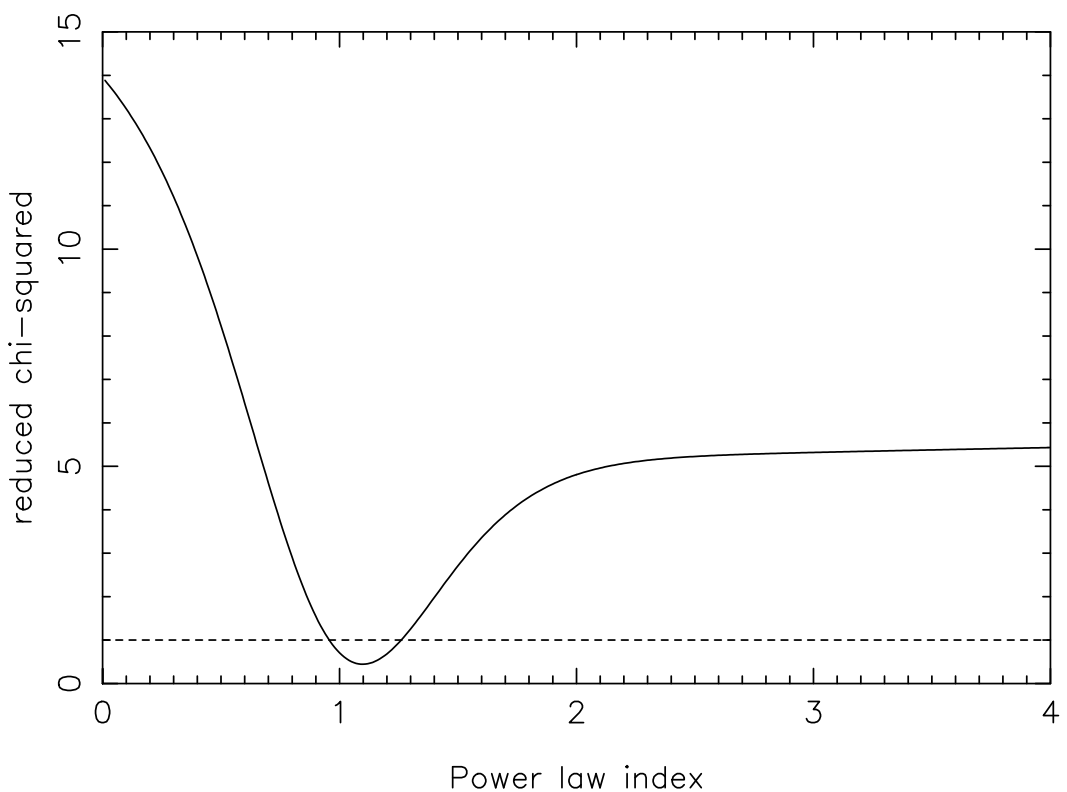


Fig. 5.— The reduced chi-squared verses power law index obtained by fitting Equation 18 to the observed number of mCVs with $P_{\text{orb}} > 3$ h.

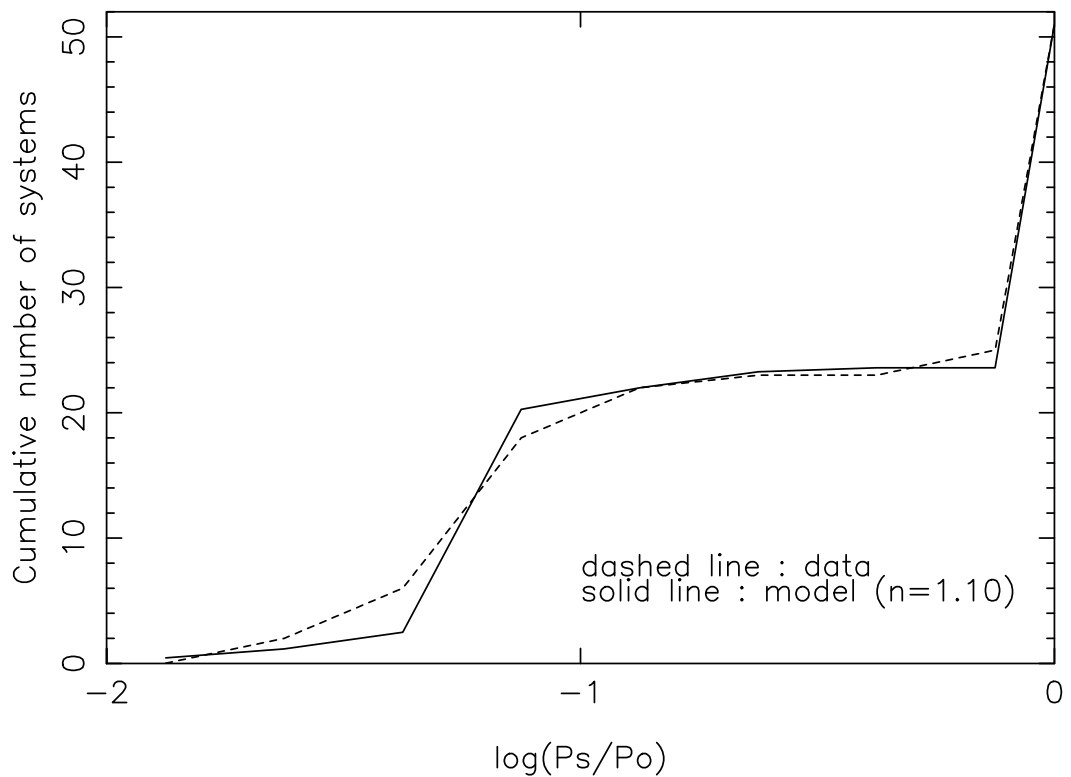


Fig. 6.— Cumulative histograms showing the observed number of mCVs with $P_{\text{orb}} > 3$ h and the predicted number according to Equation 18 with $n = 1.10$, as a function of spin to orbital period ratio.

This figure "f3.gif" is available in "gif" format from:

<http://arxiv.org/ps/astro-ph/0406363v1>